ADVANCED OPTICAL MATERIALS
www.advopticalmat.de

Plasmonic Indium Nanoparticle-Induced High-Performance Photoswitch for Blue Light Detection

*Yuan Wang, Cai-Wang Ge, Yi-Feng Zou, Rui Lu, Kun Zheng, Teng-Fei Zhang, Yong-Qiang Yu, and Lin-Bao Luo**

Plasmonic nanostructures composed of poor metals (e.g., In, Cu, Al) have lately received increasing interest due to their low cost and natural abundance relative to noble metal nanoparticles (e.g., Au, Ag, Pt). To date, while considerable progress has been achieved with regard to the utilization of plasmonic noble metal nanostructures for optimizing various optoelectronic devices, little work has been performed to study the device appplication of poor metals. In this study, a high-performance blue light nano-photodetector is induced through the use of a highly ordered indium nanoparticle (InNP) array. Electrical analysis reveals that, after decoration with the plasmonic InNP array, the photocurrent of the nano-photodetector increases considerably, giving rise to an obvious increase in responsivity and gain. Such an increase in device performance, according to simulations based on the finite element method, is attributed to the plasmonic InNPs which can induce direct electron transfer from InNPs to ZnSe nanoribbons. This study suggests that poor metal nanoparticles are equally important candidates for boosting the device performance of light-harvesting optoelectronic devices.

1. Introduction

Localized surface plasmon resonance (LSPR), commonly observed in noble metal nanostructures (e.g., Au, Ag, and Pt), is the coherent oscillation of the conduction electrons excited by an external electromagnetic irradiation.[1–3] Such a unique phenomenon has recently received tremendous research interest due to its significant role in biosensing applications such as theranostics,[4] surface-enhanced Raman spectroscopy (SERS),[5,6] and biomolecular interaction examination.[7] In addition, it has been found that the strong near-field around noble metal nanostructures derived from the LSPR will be coupled to the surrounding absorber layer and increase its absorption, leading to the effective generation of energetic hot electron–hole pairs. On this account, noble metal nanostructures have been widely employed in various optoelectronic devices and systems including solar cells,[8,9] light-emitting diodes (LEDs),[10,11] nanophotonic switches,[12–14] nanoantennas,[15,16] water splitters,[17,18] photocatalysts,[19] optical waveguides,[20] and nanolasers.[21] Although LSPR is widely observed in noble metal nanoparticles (NMNs) due to the high density of electrons, it is not limited to NMNs and can also be achieved in some poor metal nanoparticles (PMNs) including indium, tin, copper, and even aluminium with a high density of free electrons. In comparison to noble nanoparticles, the PMNs are advantageous in the following two respects: plasmonic materials made of PMNs are much cheaper to synthesize due to their natural abundance in the Earth, which make them highly competitive building blocks for various applications, and, unlikeNMNs with their tunable LSPR normally in the visible and infrared regions (AuNPs: ≈520 nm; Au nanorods: 900 nm; AgNPs: ≈460 nm), the plasmonic properties of PMNs can be readily extended across a broader electromagnetic spectrum (AlNPs: 200–250 nm, InNPs: 300–700 nm, CuNPs: 600–900 nm). In spite of the apparent advantages of plasmonic PMNs, there is a scarcity of studies about the utilization of plasmonic PMNs for various device applications, which has been successfully achieved by plasmonic NMNs. Here in this contribution, we present a novel 1D semiconductor nanostructure-based photodetector, which may find potential application in military surveillance, target detection, and light vision.[22,23] The device was composed of a highly aligned hexagonal plasmonic InNP-modified ZnSe nanoribbon (ZnSeNR)/single layer graphene (SLG) Schottky junction. Indium nanoparticles were chosen not only because they display an obvious LSPR effect like other noble metal nanoparticles (Au, Ag, and Pt), but also the LSPR band of In nanoparticles is nearly identical to the bandgap of ZnSeNR. Theoretical simulations and device analysis reveal that the InNP array can induce LSPRs which are capable of trapping incident light efficiently and enhancing the electric field near the semiconductor nanostructures, leading to enhanced photocurrents and an increase of key device parameters including responsivity and detectivity. This result suggests that plasmonic PMNs are highly competitive alternatives to boost the device performance of optoelectronic systems.

Y. Wang, C. W. Ge, Y. F. Zou, R. Lu, K. Zheng, T. F. Zhang, Dr. Y. Q. Yu, Prof. L. B. Luo
School of Electronic Science and Applied Physics and Anhui Provincial Key Laboratory of Advanced Functional Materials and Devices
Hefei University of Technology
Hefei, Anhui 230009, PR China
E-mail: luolb@hfut.edu.cn

DOI: 10.1002/adom.201500360

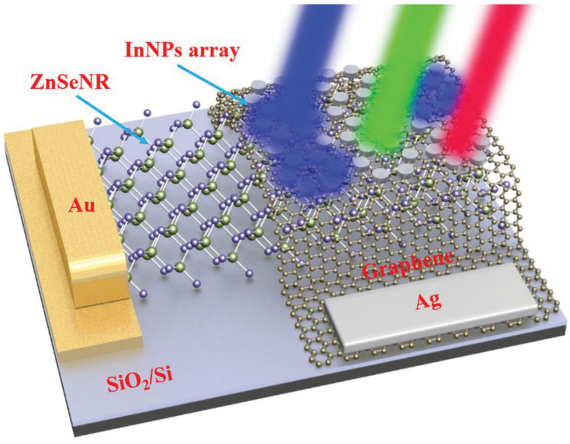

Figure 1. Schematic illustration of the blue light photoswitch based on an InNP@SLG/ZnSeNR heterojunction.

2. Results and Discussion

Figure 1 schematically illustrates the device geometry of the plasmonic nanoswitch, which consists of a highly ordered InNP-modified single-layer graphene/individual ZnSeNR Schottky junction (InNP@SLG/ZnSeNR). The hexagonally packed InNP@SLG heterostructures were fabricated by a nanosphere lithography (NSL)-assisted metal deposition approach.[24] The scheme in **Figure 2**a shows the flow chart to fabricate highly ordered InNPs. Briefly, monolayer polystyrene (PS) spheres with a diameter of 500 nm were firstly aligned on SLG, which was grown on a copper foil by chemical vapor deposition (CVD).[25] The as-assembled PS spheres were then directly coated with a layer of indium film with a thickness of ≈50 nm by electron beam evaporation. Thanks to the shading effect of the hexagonal PS spheres, the gap between them will be covered with a layer of indium metal, leading to the formation of hexagonal InNPs on the SLG. Figure 2b and c show the field-emission scanning electron microscopy (FESEM) images of the as-deposited InNP array at low and high magnifications, respectively. It is observed that all the InNPs are arranged in a hexagonal fashion, with identical distances. Moreover, the diameters of InNPs are in the range of 50–100 nm, with average value of ≈70 nm (please see the statistical distribution in the Supporting Information, Figure S1). Figure 2d shows the morphological image of the ZnSeNRs, obtained by thermal evaporation. The NRs are as long as several tens of micrometers with very smooth and clean surfaces (Figure S2). In addition, the majority of the NRs are uniform along the growth orientation. Energy dispersive spectrometry (EDS) analysis, shown in the inset, confirms that the ZnSeNRs are composed of both Zn and Se with an atomic ratio of ca. 52:48, which is very close to the compositional ratio determined by X-ray photoelectron spectroscopy (XPS, Figure S3). According to further high-resolution transmission electron microscopy (TEM) (HRTEM) and selected-area electron diffraction (SAED) studies (Figure 2e), the single crystal ZnSeNRs are in the zinc blende phase, with a growth orientation along the [200] direction. The SLG is confirmed by its Raman spectrum, which is composed of two strong peaks: one peak at 2695 cm^{-1} attributable to the 2D band, and another one at 1580 cm^{-1} due to the G-band. The intensity ratio ($I_{2D}/I_G = 2.1$) and weak band indicates the single-layer characteristic (Figure S4).

To evaluate the effect of plasmonic InNP arrays on the optoelectronic characteristics of a ZnSeNR/SLG device, we studied the device performance of ZnSeNR/SLG-based photodetectors with and without surface decoration. **Figure 3**a and b show current–voltage (I–V) curves of SLG/ZnSeNR before and after modification with hexagonally arranged plasmonic InNPs. Both devices display obvious, typical rectifying behavior. Since both ZnSeNR/Au and SLG/Ag are good ohmic contacts with negligible contact resistance, such a recrifying characteristic should be due to the formation of a Schottky junction at the ZnSeNR/SLG interface. Nevertheless, they display a virtually linear I–V characteristic when irradiated with blue light (460 nm). This finding is understandably related to the disappearance of a Schottky barrier between SLG and the NRs under light illumination.[26,27] Further photoresponses of both devices under repeated blue light illumination are shown in Figure 3c, from which one can see that both devices exhibit sensitive and reproducible photoresponses to 460 nm light irradiation that was switched on and off alternately. In comparison with the device

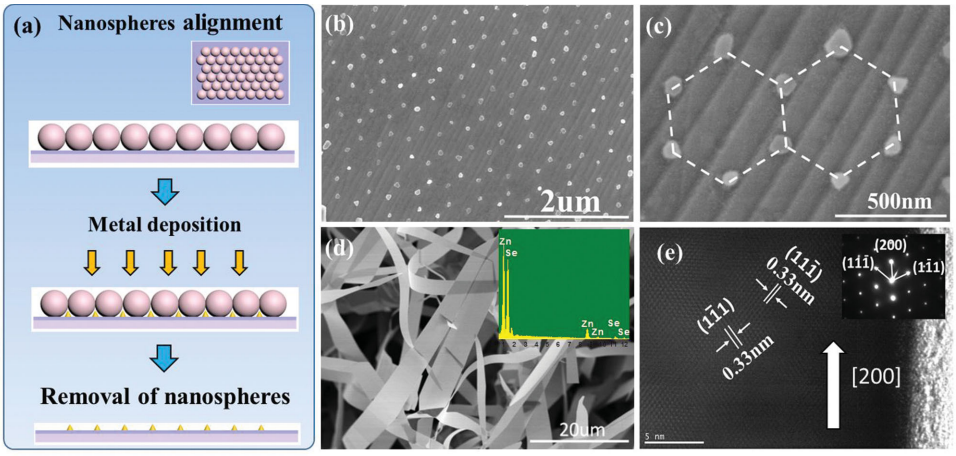

Figure 2. a) Step-wise process for the fabrication of the InNP array. Panels (b) and (c) show low- and high-magnification SEM images of the InNP array, respectively. d) FESEM image of the ZnSeNRs. The inset shows the corresponding EDS spectrum. e) HRTEM and SAED pattern of a typical ZnSeNR.

Adv. Optical Mater. **2015**,
DOI: 10.1002/adom.201500360

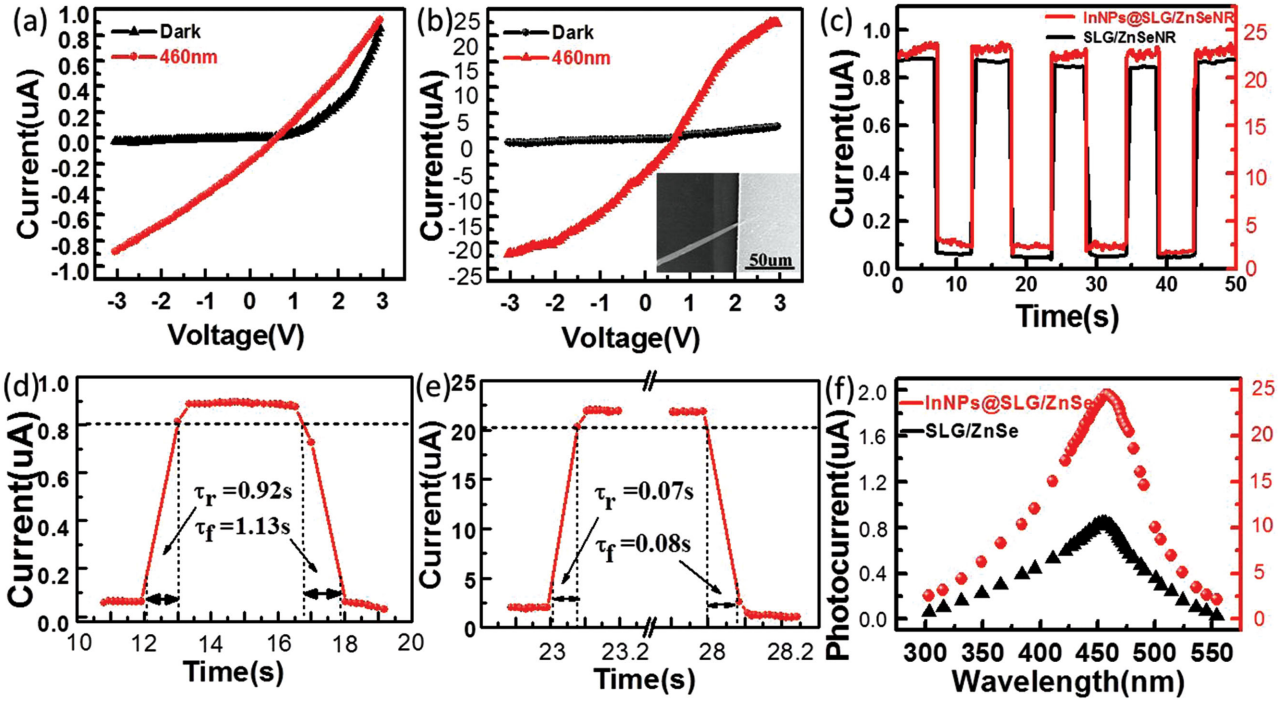

Figure 3. a) *I–V* curves of a SLG/ZnSeNR device in the dark and under light illumination. b) *I–V* curves of InNP@SLG/ZnSeNR devices in the dark and under light illumination. The measurements were conducted at room temperature. c) Photoresponse of the both devices under blue light illumination. The bias voltage was set at –3 V. d) One cycle photoresponse of the SLG/ZnSeNR device. e) One cycle photoresponse of the InNP@SLG/ZnSeNR device. f) Spectral response of both devices.

without InNPs, the photocurrent of the device with InNPs is substantially increased by 20-fold, from 0.9 to 22 μA at a bias voltage of –3 V. In addition to the enhancement in photocurrent, decoration with plasmonic InNPs can bring about a faster response rate as well. Figure 3d and e show the response times of both devices to blue light illumination. The rise time (t_r) and fall time (t_f) for SLG/ZnSeNR devices are derived to be 0.92 and 1.13 s, respectively, which are much slower than that of InNP@SLG/ZnSeNR devices (t_r: 0.07 s and t_f: 0.08 s). Although the underlying origin for this enhancement in response rate is still unclear and needs further investigation, a similar observation has been reported in noble metal nanoparticle-decorated photodetectors as well.[28] The last but not least advantage of the current plasmonic photoswitch is that the decoration with the InNPs will not result in extra spectral sensitivity. The spectral response of the both devices in Figure 3f reveals good spectral selectivity, with a peak sensitivity at ≈460 nm. Such a consistency in spectral response relates to perfect agreement of the bandgap of the ZnSeNRs (≈460 eV),[29] and the LSPR band of the InNPs (≈460 nm), which is estimated by theoretical simulations.

Table 1. Device performance comparison of SLG/ZnSeNR, InNP@SLG/ZnSeNR, and other ZnSe nanostructure-based devices.

Material	R [A W^{-1}]	G	Response time [s]	Reference
SLG/ZnSeNR	26.5	71.6	<2	Our work
InNP@SLG/ZnSeNR	6.47×10^2	1.75×10^3	<0.1	Our work
ZnSe nanobelt	0.12	–	0.3	[30]
ZnSe nanowire	22.0	–	–	[31]

In order to quantitatively assess the effect of plasmonic InNP arrays on the device performance of blue-light photoswitches, the responsivity (R) is calculated using the following equation:[30] $R = I_p/P_{opt} = \eta G q\lambda/hc$, where I_p, P_{opt}, η, λ, h, c, and G denote the photocurrent, incident light power, quantum efficiency, light wavelength, Planck's constant, light speed, and the photoconductive gain, respectively. By assuming $\eta = 1$ for convenience, R is estimated to be 26.5 and 6.47×10^2 A W^{-1} for SLG/ZnSeNR and InNP@SLG/ZnSeNR, respectively. What is more, the G of the InNP@SLG/ZnSeNR device is calculated to be 1.75×10^3, much higher than that of the SLG/ZnSeNR device (71.6). **Table 1** summarizes the performances of current blue-light photodetectors and other devices based on ZnSe nanostructures. It is easy to note that, after decoration with InNPs, both G and R are not only higher than that of the SLG/ZnSeNR device, but also higher than that of other ZnSe nanostructure-based photodetectors, including ZnSe nanobelts[31] and ZnSe nanowires.[32] As will be discussed later, the relatively high performance of our InNP@SLG/ZnSeNR device is due to the contribution from the plasmonic InNPs that can induce direct electron injection from InNPs to SLG under 460 nm light illumination.

Figure 4a compares the experimental absorption of both InNP@SLG/ZnSeNR and SLG/ZnSeNR. It is clear that, compared with SLG/ZnSeNR, the absorption intensity of InNP@SLG/ZnSeNR is relatively strong in the range 400–600 nm. Such an increase in absorption is due to the presence of the In

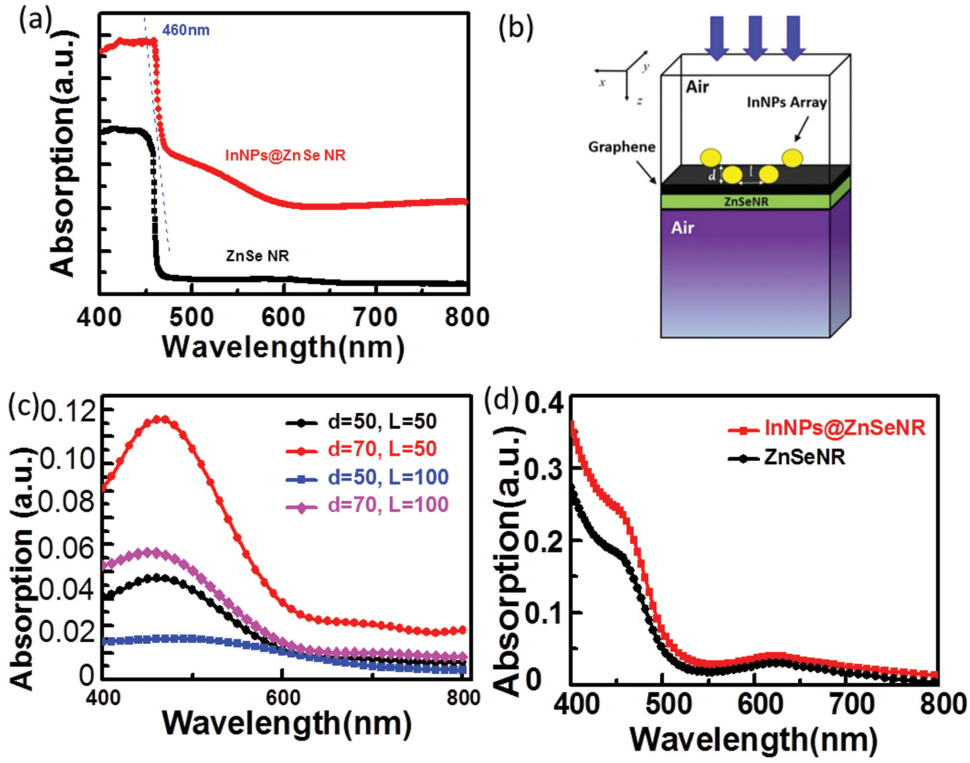

Figure 4. a) Experimental absorption spectra collected from both ZnSeNRs and InNP array-modified ZnSeNRs. b) Schematic diagram of model used in simulation. c) Theoretical absorption of the InNPs with the different lattice constants (*l*) and diameters (*d*). d) Theoretical absorption spectra of both ZnSeNRs and InNP array-modified ZnSeNRs.

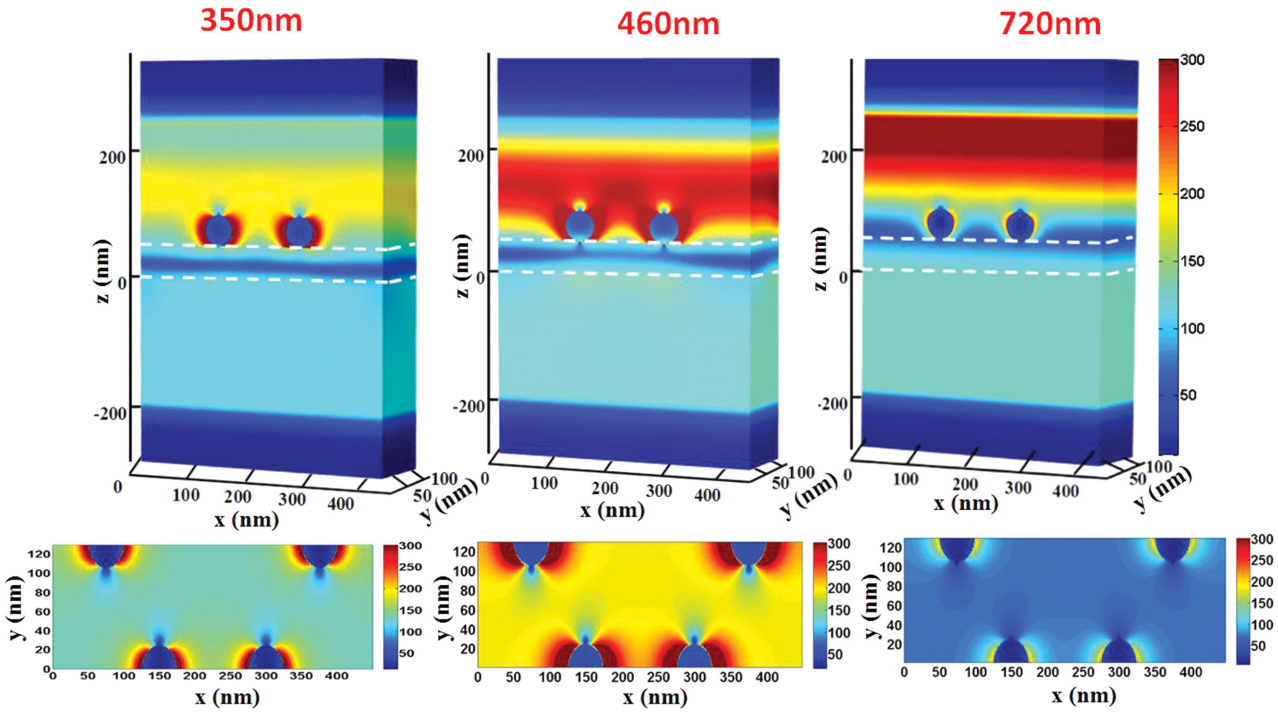

Figure 5. The upper row of plots are 3D electric field energy-density distributions of the SLG/ZnSeNRs decorated with plasmonic InNPs under light illumination with wavelengths of 350, 460, and 720 nm, repectively. The diameters of all InNPs are 50 nm. The lower row of plots are the electric field energy-density distribution on the cross-section of plane Z = 0.

Adv. Optical Mater. **2015**,
DOI: 10.1002/adom.201500360

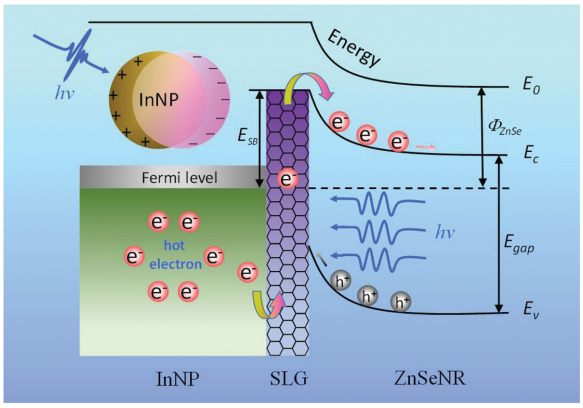

Figure 6. Band diagram of the plasmonic InNP-decorated photodetector under blue light illumination.

nanoparticles that can increase the optical path length inside the semiconductor to effectively trap incident light. As a result, the light absorption of the metal nanoparticle/semiconductor nanostructure hybrid was increased. In order to unveil the optical properties of SLG/ZnSeNR modified with the hexagonal InNP array, theoretical simulations of the plasmonic InNPe were performed using the finite element method (FEM). Basically, the model is composed of ZnSeNR in close contact with SLG, on which a hexagonal InNP array is placed (Figure 4b). The density and size of InNPs are determined by their lattice constant (l) and diameter (d), respectively (Figure S5). For convenience, the absorption of pure InNPs was firstly considered. Figure 4c depicts the theoretical absorption spectrum of InNPs with different l and d. It is seen that all the NPs exhibit obvious light absorption at 460 nm, which can be attributed to the LSPR band of the InNPs according to a previous study.[33] What is more, among the three kinds of InNPs considered in our simulation, the NPs with d = 70 nm and l = 50 nm exhibit the strongest light absorption, which means InNPs with larger diameter and higher density could result in stronger absorption. In addition to lattice constant and diameter, the LSPR band is dependent on the thickness of the InNPs (Figure S6). Notably, further theoretical simulations find that the modification of the SLG/ZnSeNR Schottky junction with plasmonic InNPs will cause an obvious increase in light absorption in the region 400–500 nm (Figure 4d). As a matter of fact, the excitation of the LSPR is further verified by theoretical simulations based on FEM. **Figure 5** shows the 3D electric field distributions of the InNP array under light illumination with wavelengths of 350, 460, and 720 nm. The 50 nm InNPs can induce a large-area and relatively strong enhancement in electric energy (hot spots) at a wavelength of 460 nm, which is close to the LSPR wavelength of InNPs. Decreasing or increasing the illumination wavelength, however, leads to a relatively weak enhancement in energy. This selectivity in excitation wavelength agrees well the peak sensitivity at 460 nm.

The high sensitivity of the present plasmonic blue light photodetector is associated with its unique operation mechanism. As shown in **Figure 6**, the SLG/ZnSeNR device is characterized by a depletion region (or built-in electric field) at the SLG/ZnSeNR interface, as a result of band bending due to their difference in work functions. The as-formed depletion region can efficiently separate photogenerated electron–hole pairs when irradiated with blue light, giving rise to a photocurrent in the circuit. Such a process corresponds to the detection mechanism of the SLG/ZnSeNR device. Significantly, the generation of photocurrent can be favorably facilitated when plasmonic InNPs are attached onto the surface of the SLG. In this case, the photocurrent under light illumination is composed of two parts. The first part is associated with the photocurrent formed at the SLG/ZnSeNR interface. The second part is due to the plasmonic InNP-induced hot electron injection. Upon 460 nm illumination, the InNPs, like other noble metal nanoparticles, are able to trap incident light and induce LSPR.[34–36] The resultant energetic electrons (also termed hot electrons) within the InNPs can easily transfer to the nearby SLG with a relatively high energy.[37] The injected electrons at the SLG migrate to the SLG/ZnSeNR interface, and are then separated by the depletion region. It is worth noting that, due to the high quality of the ZnSeNRs (smooth and clean surfaces with large areas), the InNP-decorated SLG film can form a tight contact with the underlying NRs. Such a special device configuration is highly helpful to electron injection, and therefore is beneficial to the device performance of the InNP@SLG/ZnSeNR device.

3. Conclusion

We have presented a plasmonic blue-light photoswitch by modifying a SLG/ZnSeNR Schottky junction with poor metal nanoparticles (InNPs). Electrical analysis reveals that, after decoration with the InNP array, the photocurrent increased considerably by nearly 20-fold, from 0.9 to 22 μA, giving rise to an obvious increase in response and gain. The high performance, according to our theoretical simulations based on FEM, is due to the LSPR-induced direct electron injection from InNPs to SLG, followed by separation by a built-in electric field. This study suggests that plasmonic nanoparticles composed of poor metals are important alternatives to boost the performance of optoelectronic devices.

4. Experimental Section

Synthesis and Structural Study of ZnSe Nanoribbons and Hexagonal InNP Array@MLG: Briefly, monolayer graphene (MLG) films were firstly prepared via CVD using CH_4 and H_2 as reaction sources, and 25 μm-thick Cu foils as a catalytic substrate. To fabricate the hexagonal InNP array@SLG architecture, monolayer polystyrene (PS) spheres (diameter: 500 nm) were firstly self-assembled onto a graphene film on copper foil by drop-coating. The close-packed monolayer PS spheres were transformed into a non-close-packed arrangement by reactive ion etching (RIE), during which the oxygen gas was kept at a flow rate of 20 standard cubic centimeters per minute (SCCM) , and the RF power was set at 50 W. Afterwards, a 50 nm-thick indium film was deposited on the non-close-packed PS spheres by thermal evaporation, followed by the removal of the PS spheres in a hot alcohol solution (about 50 °C) for 10 min. Finally, the sample was rapidly stirred in toluene solution, via which the PS spheres were removed rapidly. The ZnSe nanoribbons were synthesized by thermal evaporation of pure ZnSe powder at 1050 °C in a horizontal tube furnace via a conventional vapor–liquid–solid (VLS) process. The morphology of the hexagonal InNP arrays and ZnSeNRs

were characterized by field-emission scanning electron microscopy (FESEM, SIRION 200 FEG), and high-resolution transmission electron microscopy (HRTEM, JEOL JEM-2100F). The Raman study of MLG was carried out on a Raman spectrometer (JY, LabRAM HR800). The chemical composition of the as-fabricated ZnSeNR was analyzed by X-ray photoelectron spectroscopy (XPS, Thermo ESCALAB 250).

Device Fabrication and Characterization: To fabricate the plasmonic photodetector, photolithography and electron beam evaporation were used to define single Au (50 nm) electrodes on ZnSeNRs which were dispersed on a SiO_2 (300 nm-thick)/Si substrate in a parallel fashion by contact printing. The remaining photoresist was removed by a simple lift-off process. Then, an MLG film decorated with a InNP array was transferred onto the other head of the ZnSeNR. Last, silver paste was placed onto the graphene to facilitate further device analysis. The optoelectronic characteristics of the plasmonic photodetector were conducted at room temperature by using a semiconductor characterization system (Keithley 4200-SCS) and a monochromatic light source system.

Theoretical Simulations: the numerical electromagnetic calculations were performed using the finite element method (FEM). In view of the periodic structural model, the computational domain only contained a unit cell, and perfect electric conductors (PECs) and perfect magnetic conductors (PMCs) were employed for four lateral boundaries. Perfectly matched layers were applied in the propagation directions to eliminate nonphysical boundary reflections. When a plane wave with polarization along the *x*-axis normally irradiated the planar structure, the light absorption of ZnSeNRs was calculated by the following expression: $A = 1 - R - L - T$, where A is the absorption in ZnSeNRs, R is the total reflectance, T is the total tranmitance, and L is the total loss in the InNPs. The optical data of SLG was obtained from the $\sigma 0$ model.[38] The optical data of ZnSe was from the database of Sopra S. A. Company, and In was extracted from Luxpop.

Acknowledgements

This work was supported by the Natural Science Foundation of China (NSFC, Nos. 21501038, 61575059, 21101051), the Natural Science Foundation of Anhui Province (Grant No. J2014AKZR0059), and the Fundamental Research Funds for the Central Universities (2011HGZJ0004, 2012HGCX0003, 2013HGCH0012, 2014HGCH0005).

Received: June 28, 2015
Revised: August 24, 2015
Published online:

[1] K. A. Willets, R. P. Van Duyne, *Annu. Rev. Phys. Chem.* **2007**, *58*, 267.
[2] C. Noguez, *J. Phys. Chem. C.* **2007**, *111*, 3806.
[3] K. L. Kelly, E. Coronado, L. L. Zhao, G. C Schatz, *J. Phys. Chem. B.* **2003**, *107*, 668.
[4] E. C. Dreaden, A. M. Alkilany, X. H. Huang, C. J. Murphy, M. A. ElSayed, *Chem. Soc. Rev.* **2012**, *41*, 2740.
[5] J. F. Li, Y. F. Huang, Y. Ding, Z. L. Yang, S. B. Li, X. S. Zhou, F. R. Fan, W. Zhang, D. Y. Wu, *Nature* **2010**, *464*, 392.
[6] L. B. Luo, L. M. Chen, M. L. Zhang, Z. B. He, W. F. Zhang, G. D. Yuan, W. J. Zhang, S. T. Lee, *J. Phys. Chem. C.* **2009**, *113*, 9191.
[7] S. C. Gopinath, P. K. Kumar. *Analyst* **2014**, *139*, 2678.
[8] H. A. Atwater, A. Polman, *Nat. Mater.* **2010**, *9*, 205.
[9] H. R. Tan, R. Santbergen, A. H. M. Smets, M. Zeman, *Nano Lett.* **2012**, *12*, 4070.
[10] A. Kock, E. Gornik, M. Hauser, W. Beinstingl, *Appl. Phys. Lett.* **1990**, *57*, 2327.
[11] K. Okamoto, I. Niki, A. Shvartser, Y. Narukawa, T. Mukai, A. Scherer, *Nat. Mater.* **2004**, *3*, 601.
[12] L. B. Luo, X. L. Huang, M. Z. Wang, C. Xie, C. Y. Wu, J. G. Hu, L. Wang, J. A. Huang, *Small* **2014**, *10*, 2645.
[13] C. H. Hsieh, L. J. Chou, G. R. Lin, Y. Bando, D. Golberg, *Nano Lett.* **2008**, *8*, 3081.
[14] L. B. Luo, W. J. Xie, Y. F. Zou, Y. Q. Yu, F. X. Liang, Z. J. Huang, K. Y. Zhou, *Opt. Exp.* **2015**, *23*, 12979.
[15] B. J. Roxworthy, K. D Ko, A. Kumar, K. H. Fung, E. K. C. Chow, G. L. Liu, N. X. Fang, K. C. Toussaint, *Nano Lett.* **2012**, *12*, 796.
[16] W. J. Yao, S. Liu, H. M. Liao, Z. Li, C. W. Sun, J. J. Chen, Q. H. Gong, *Nano Lett.* **2015**, *15*, 3115.
[17] D. B. Ingram, S. Linic, *J. Am. Chem. Soc.* **2011**, *133*, 5202.
[18] W. T. Kung, Y. H. Pai, Y. K. Hsu, C. H. Lin, C. M. Wang, *Opt. Exp.* **2013**, *21*, 221.
[19] E. Kowalska, O. O. P. Mahaney, R. Abe, B. Ohtani, *Phys. Chem. Chem. Phys.* **2010**, *12*, 2344.
[20] M. Wu, Z. H. Vien Van, *Opt. Exp.* **2010**, *18*, 11728.
[21] C. Y. Wu, Kuo, C. T. Wang, C. Y. He, C. L. Lin, M. H. Ahn, H. S. Gwo, *Nano Lett.* **2011**, *11*, 4256.
[22] Z. X. Wang, M. Safdar, M. Mirza, K. Xu, Q. S. Wang, Y. Huang, F. M. Wang, X. Y. Zhan, J. He, *Nanoscale* **2015**, *7*, 7252.
[23] Z. X. Wang, M. Safdar, C. Jiang, J. He, *Nano Lett.* **2012**, *12*, 4715.
[24] L. B. Luo, J. J. Chen, M. Z. Wang, H. Hu, C. Y. Wu, Q. Li, L. Wang, J. A. Huang, F. X. Liang, *Adv. Funct. Mater* **2014**, *24*, 2794.
[25] F. Wang, Z. X. Wang, Q. S. Wang, F. M. Wang, L. Yin, K. Xu, Y. Huang, J. He, *Nanotechnology* **2015**, *26*, 292001.
[26] K Keem, H. Kim, G. T. Kim, J. S. Lee, B. Min, K. Cho, M. Y. Min, S. Kim, *Appl. Phys. Lett.* **2004**, *84*, 4376.
[27] B. Nie, J. G. Hu, L. B. Luo, C. Xie, L. H. Zeng, P. Lv, F. Z. Li, J. S. Jie, M. Feng, C. Y. Wu, Y. Q. Yu, S. H. Yu, *Small* **2013**, *17*, 2872.
[28] K. W. Liu, M. Sakurai, M. Y. Liao, M. Aono, *J. Phys. Chem. C.* **2010**, *114*, 19835.
[29] B. Nie, L. B. Luo, J. J. Chen, J. G. Hu, C.Y. Wu, L. Wang, Y. Q. Yu, Z. F. Zhu, J. S. Jie, *Nanotechnology* **2013**, *24*, 095603.
[30] Z. X. Wang, K. Xu, Y. C. Li, X. Y. Zhan, M. Safdar, Q. S. Wang, F. M. Wang, J. He, *ACS Nano* **2014**, *8*, 4859.
[31] X. S. Fang, S. L. Xiong, T. Y. Zhai, Yoshio. Bando, M. Y. Liao, Ujjal. K. Gautam, Y. Koide, X. G. Zhang, Y. T. Qian, D. Golberg, *Adv. Mater.* **2009**, *21*, 5016.
[32] J. Salfi, U. Philipose, C. F. D. Sousa, *Appl. Phys. Lett.* **2006**, *89*, 261112.
[33] Y. C. Chang, C. B. Tseng, *Plasmonics* **2013**, *8*, 1395.
[34] A. Pescaglini, A. Martin, D. Cammi, G. Juska, C. Ronning, E. Pelucchi, D. Iacopino, *Nano Lett.* **2014**, *14*, 6202.
[35] A. George, H. K. Choudhary, B. Satpati, S. Mandal, *Phys. Chem. Chem. Phys.* **2015**, *17*, 7109.
[36] N. Esser, A. M. Frisch, A. Roseler, S. Schintke, C. Goletti, B. O. Fimland, *Phys. Rev. B* **2003**, *67*, 125306.
[37] S. Linic, P. Christopher, D. B. Ingram, *Nat. Mater.* **2011**, *10*, 911.
[38] G. Isic, M. Jakovjevic, M. Filipovic, D. Jovanovic, B. Vasic, S. Lasovic, N. Puac, Z. L. Petrovic, R. Kostic, R. Gajic, *J. Nanophotonics* **2011**, *5*, 051809.